ACTA CHEMICA IASI, **34_2**, 377-404 (2026)
DOI: 10.47743/achi-2026-2-0016

Article

L9 ORTHOGONAL VALIDATION ON THE DISSOLUTION BEHAVIOR OF RECYCLED COTTON AND POLYESTER IN PURE DMSO FROM MOLECULAR DYNAMICS SIMULATION PREDICTION

Arbanah Binti Muhammad[a*], Nur Ummul Waliyyatullah Muhammad Faez Tan[a], Noor Fitrah Abu Bakar[b], Intan Suhada Azmi[a] and Azmi Roslan[a]

[a]*Faculty of Chemical Engineering, Universiti Teknologi MARA, Johor Branch, Pasir Gudang Campus, 81750 Masai, Johor, Malaysia.*

[b]*Faculty of Chemical Engineering, Universiti Teknologi MARA, 40450, Shah Alam, Selangor, Malaysia.*

Abstract: Molecular Dynamics (MD) simulation was used to investigate polymer-solvent interactions, predicting that cotton (cellulose) exhibits stronger interactions with Dimethyl Sulfoxide (DMSO) at 423 K(150°C) and 4.5 mg/mL compared to polyester (PET). These predictions were validated experimentally using an L9 orthogonal array to optimize temperature, polymer concentration and dissolution time for effective dissolution while preserving structural integrity. Optimal conditions (150°C, 4.5 mg/mL, and 8 h) yielded ~80% cotton dispersion efficiency versus <20% for PET with the most significant condition of temperature ($P<0.05$). Applying these conditions to of polycotton blends achieved selective cotton dispersion with similar high efficiency. Structural characterization of water-regenerated cotton via anti-solvent precipitation confirmed that crystallinity, functional groups, and morphology remained comparable to pure cotton, indicating an intact cellulose backbone. To evaluate the quality of regenerated

[*]Arbanah Muhammad, *e-mail*: arbanah7188@uitm.edu.my

cotton, the dispersed cellulose was regenerated using water through an anti-solvent precipitation method. The structural characterisation indicated that the regenerated cotton maintained comparable crystallinity, functional groups, and morphological with pure cotton, indicating an intact cellulose backbone. Overall, DMSO serve as an effective single solvent for selective cotton dispersion and polycotton separation, demonstrating MD simulation as viable tool for optimizing polymer-solvent systems.

***Keywords*:** Molecular Dynamic Simulation, Cotton, Dissolution, Recycled Textile, Dimethyl Sulfoxide

Introduction

Molecular Dynamics (MD) simulation are frequently applied to validate experimental data rather than predict outcomes, particularly polymer-solvent interactions.[1] This underutilizes MD, which is designed to investigate atomic-level interactions before laboratory testing.[2] Furthermore, MD prediction for polymer-solvent dissolution are often restricted to temperature and concentration effects. Yan et al. showed that cellulose requires a lower activation energy (14.81 kcal/mol) for dissolution than polyester (21.46 kcal/mol) across varying temperature, concentration and dissolution time.[3] Wu et al., further noted that these parameters drive dissolution by directly disrupting intra- and intermolecular hydrogen bonds to cleave polymer chains.[4] Thus, integrating computational and experimental methods is essential to optimize system performance reliably.

The Taguchi L9 orthogonal array method is a reliable optimization technique that provide statistical evaluation to identify individual parameter effects and improve experimental consistency approach for optimization.[5,6] Consequently, it is ideal for dissolution studies to determine how factors like temperature, polymer concentration, and dissolution time influence polymer–solvent interactions while minimizing experimental error.[7] However, dissolving blended fibers like cotton-polyester remains a key

bottleneck in textile recycling. While dissolution-based recycling offers high efficiency, its application is constrained by significant environmental and safety drawbacks.[8] In particular, most solvents capable of dissolving cotton and polyester pose notable hazardous.[9]

Previous studies have mostly focussed on dissolution using dimethyl sulfoxide (DMSO) as co-solvent, where the solvent mixture typically contains a higher DMSO proportion. For instance, Ren et al. (2021) used ionic liquid (IL) and DMSO mixtures at 1:2 mole rations, achieving the highest average cellulose dissolution efficiency up to 15 wt%.[10] This suggests that DMSO enhances the disruption of intermolecular hydrogen bonding within the cellulose structure and improves the dissolution process, indicating that DMSO plays dominant role in facilitating the dissolution. However, IL-DMSO solvent system raises concerns regarding recyclability and sustainability, as ILs are often associated with high cost and complex recovery. Furthermore, pure DMSO is highly polar and non-toxic, with the ability to form hydrogen bonds or dipole-dipole interactions.[11] Its potential as a neat solvent is further supported by its thermal stability up to 189 – 190 °C, though it decomposes at higher temperatures to release sulphur compounds.[12]

Furthermoe, polymer–solvent interactions depend primarily on concentration and temperature, which govern solvation free energy, chain mobility, and phase stability.[13] Solvent characteristics, particularly polarity, dictate assembly. DMSO was chosen for this study because of its in high polarity, low toxicity, and amphiphilic character. Containing polar (sulfoxide) and nonpolar (methyl) functional groups, DMSO offers a promising replacement for hazardous solvents.[14,15] To date, limited research exists on molecular interaction mechanisms governing cotton and polyester

dissolution in pure DMSO.[16] This study evaluates pure DMSO as a primary solvent for dissolving textiles waste.

Most studies focus on the dissolution process while overlooking the structural verification of regenerated cellulose, leaving textile circularity incompletely addressed. Among recovery techniques, anti-solvent precipitation is ideal for regeneration cellulose from solvent mixtures. Using water as an anti-solvent drives the transition from cellulose I(parallel chains) to cellulose II(antiparallel chains).[17,18] While cellulose I offer superior mechanical strength, cellulose II provides greater chemical reactivity and thermodynamic stability, facilitating key industrial applications such as mercerization and recycling.[19,20] Excess water competes with DMSO for hydrogen bonding, driving rapid solid precipitation and increasing regeneration yield.[21,22] Together, these mechanism dictate the structural quality and mechanical performance for regenerated fibers.

Few studies have comprehensively validated MD simulation predictions through experimental optimization of cotton and polyester dissolution in pure DMSO. In this study, MD simulations are first employed to predict the molecular interactions of cotton and polyester with pure DMSO. Dissolution is subsequently optimized using L9 orthogonal array to identify the optimal operating conditions. The regenerated fibres are then characterized for their structural, thermal and morphological properties to evaluate quality preservation of fiber quality. This integrated approach establishes a closed-loop textile recycling strategy that combines solvent sustainability with fiber-quality preservation for practical solution in circular textile economy.

Results and Discussion

Prediction by MD Simulation

Dissolution parameters (concentration, time and temperature) were evaluated to assess their impact on solvent-polymer interaction, solvent penetration, chain mobility and structural evaluation. Concentration effect was modelled using binding energy, interaction energy, and MSD (Figure 1). At 4.5mg/mL, both cellulose and PET systems showed a pronounced MSD fluctuations, reflecting significant atomic displacement from polymer-solvent engagement (Figure 1 (a) and (b).[23] This suggests that elevated concentrations restrict segmental mobility and chain entanglement. This behavior underscores PET's low compatibility with polar aprotic solvents like DMSO, owing to its semi-rigid aromatic backbone and sparse polar interaction sites.[24] In contrast, the cellulose/DMSO system displayed double the MSD of PET/DMSO. The difference arises because cellulose hydroxyl groups readily interact with polar DMSO molecule to accelerate solvent penetration and disrupt intermolecular hydrogen bonds. In contrast, the DMSO preferentially interacts with the PET's ester and carbonyl groups leading to molecular interaction behaviour distinct from the cellulose.

As shown in Figure 1 (c), the PET/DMSO system exhibited more negative interaction energy than cellulose/DMSO system, indicating a stronger polymer-solvent affinity. However, favourable interaction energy alone is insufficient for complete dissolution, which also requires DMSO to penetrate the polymer matrix and overcome cohesive PET-PET interactions. PET's rigid aromatic backbone restricts chain mobility and solvent penetration, ultimately limiting dissolution despite the favourable PET-DMSO interaction.

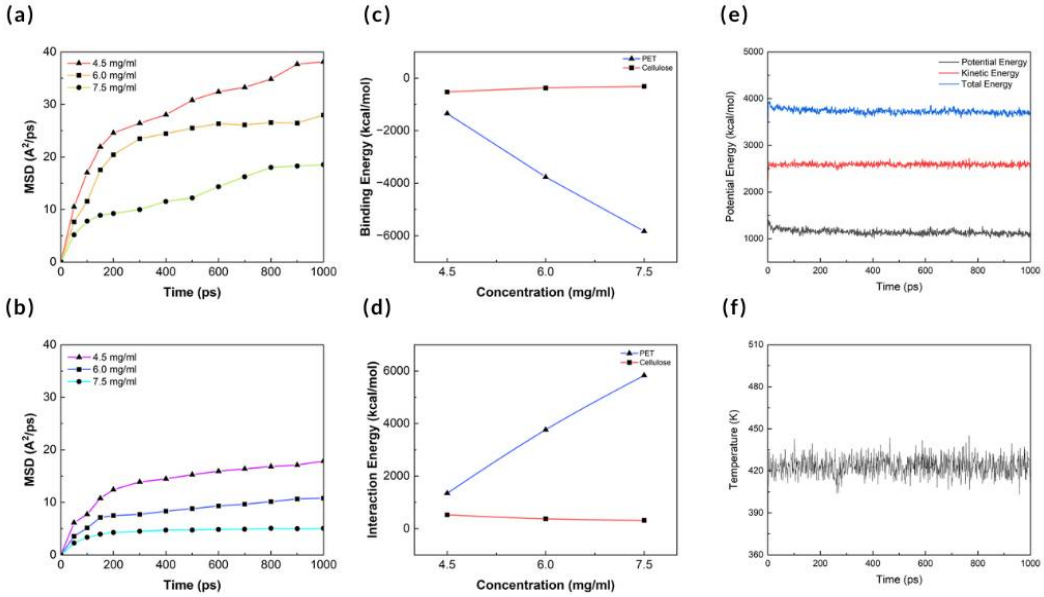


Figure 1. MSD graph of (a) PET-DMSO (b) Cellulose-DMSO, (c) Binding Energy, (d) Interaction Energy, (e) Temperature Curve, (f) Energy Curve of Equilibration System throughout the 1000 ps Trajectory.

In contrast, Figure 1(d) shows a less negative interaction energy for the cellulose/DMSO system, which does not necessarily indicate reduced dissolution potential. Instead, cellulose's hydroxyl-rich structure forms specific hydrogen bonds with DMSO that disrupt inter-and intramolecular networks, promoting chain separation and solvent penetration. Interaction energy must therefore be interpreted alongside structural and dynamic system properties rather than as a direct proxy for dissolution performance. MD simulations predicted peak solvation at 4.5 mg/mL and 423K which also represent the optimal simulated conditions. This aligns with findings by Cheng et al., who reported that overly strong polymer-solvent interaction energies can impede solvent diffusion, thereby decreasing solvent mobility and availability.[25] The findings are summarized in Table 1.

Table 1. Summary of molecular interaction studies.

MD parameter	Cellulose (cotton)	PET	Interpretation
Binding energy	Approximately 500 to 350 kcal/mol (relatively small variation with concentration)	Increase substantially from 1400 to 5800 kcal/mol as concentration increases	PET exhibits a much stronger concentration-dependent energetic association with DMSO
Interaction energy	Decrease slightly from 500 to 300 kcal/mol	Increase markedly from 1300 to 5800 kcal/mol	DMSO-PET interaction is considerably more sensitive to DMSO concertation
MSD	MSD decreases with increasing concentration	MSD decreases with increasing concentration	Higher concentration is associated with reduced molecular mobiliy/greater molecular association
Concentration effect	Relatively weak change in energetic interaction	Strong change in energetic interaction	Concentration has more pronounced effect on PET than cellulose
Simulation stability	Reaches equilibrium rapidly with minimal energy fluctuation	Maintains structural and energetic equilibrium throughout simulation	Potential, kinetic and total energies remain relatively stable across both polymer system
Temperature	Stable solvation and enhanced chain mobility from 300K to 423 K	Limited solvent diffusion and restricted mobility from 300K to 423K	Temperature elevation selectively promotes solvent penetration and chain mobility in cellulose over PET
Overall molecular response	Relatively stable interaction with DMSO across concentration	Strong concentration-dependent interaction with DMSO	Demonstrates distinctly different molecular responses of cellulose and PET toward DMSO

Dissolution Process Validation

The dissolution behaviour of cellulose and PET evaluated via L9 orthogonal design (50 – 150 ℃, 4.5 – 7.5 mg/mL, 4-8 h) is shown in Figure 2. Cellulose achieved a peak dissolution ~80% under condition E7 (150 ℃, 4.5 mg/mL, 8 h) whereas lower temperatures yielded only 24 – 33 %

(50 °C) and 35–41 % (100°C). Increasing the concentration beyond 4.5 mg/mL 150 °C, reduced cellulose dissolution to 66 % (E8) and 64 % (E9). PET showed consistently poor dissolution across all conditions, peaking at just 13 % at E7. These results underscore the strong temperature dependence of dissolution, as thermal energy enhances chain mobility and solvent penetration. However, higher polymer concentration hinders dissolution, necessitating balanced process parameters. Cellulose dissolved effectively because its abundant hydroxyl (-OH) groups form strong interactions with DMSO's polar sulfoxide group, accelerating swelling and chain disentanglement.[26,27] Conversely, PET's rigid, hydrophobic aromatic backbone restricts solvent penetration and chain separation, consistent with observation by Ren et al. (2021). It further facilitates solvent-polymer interactions, chain disentanglement, and swelling.[28,29,30] These experimental trends align directly with MD predictions (420K), confirming distinct solvent interaction and mobility profiles for cellulose verses PET in DMSO.

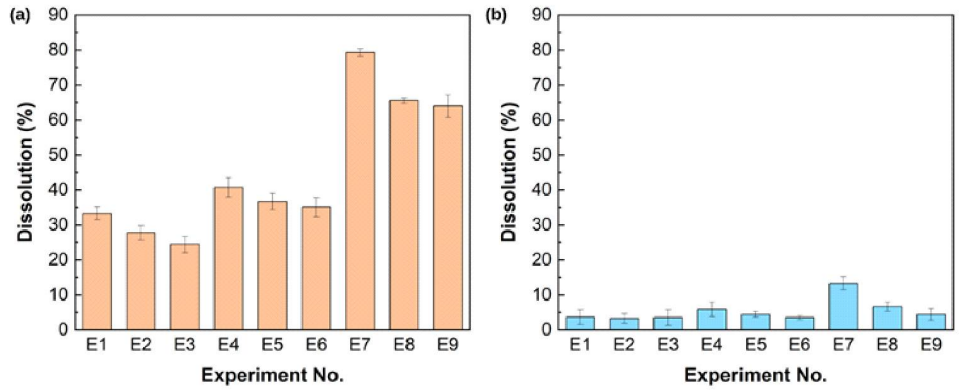


Figure 2. The result of varying conditions on (a) cotton, (b) polyester dissolution in DMSO.

The statistical significance of temperature, concentration, and dissolution time was evaluated using ANOVA (Table 2) and S/N main effects plots (Figure 3). For cellulose, temperature was the sole statistically significant

factor (F= 148.17, P < 0.05), while concentration (F= 53.03, P > 0.05) and time (F= 1.86, P= 0.349) has negligible effects. Temperature was likewise the only significant variable for PET (F= 22.42, P<0.005), with concentration (F= 12.45, P > 0.05) and time (F= 5.84, P= 0.146) remaining non-significant at the 95% confidence level. S/N ratio main effects plots confirm temperature as dominant parameter, displaying the largest mean variation across evaluated levels.

Table 2. Analysis of Variance (ANOVA) for SN ratios for cotton and polyester.

	Cotton				**Polyester**			
	SSk	**MSk**	**F value**	**Reporting**	**SSk**	**MSk**	**F value**	**Reporting**
Temperature (°C)	1.373	0.687	148.17	P < 0.05	46.50	23.25	22.42	P < 0.05
Concentration (mg/mL)	0.492	0.246	53.03	P > 0.05	25.83	12.92	12.45	P > 0.05
Dissolution Time (h)	0.017	0.009	1.86	P = 0.349	12.10	6.05	5.84	P = 0.146
Residual Error	0.009	0.005			2.074	1.04		
Total (SST)	1.892				86.51			

These findings align with experimental results (Figure 2), where elevating temperature from 50 to 150 °C dramatically increased cellulose dissolution. PET followed a similar temperature-dependent response but achieved much lower overall dissolution.

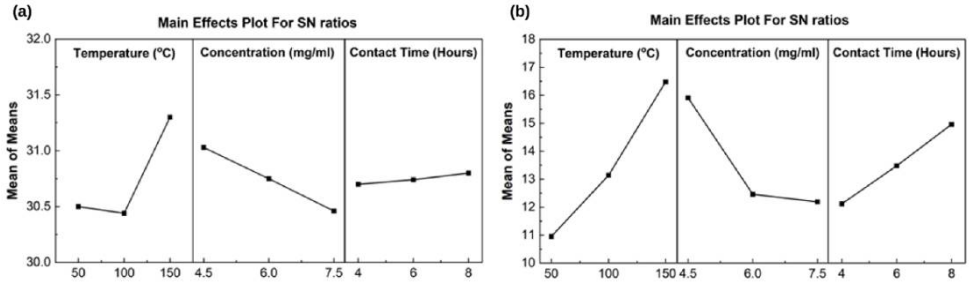


Figure 3. Main Effect Plot for S/N ratios for (a) cotton and (b) polyester.

This confirms that DMSO effectively disrupts cellulose's hydrogen-bonded network to promote chain mobility and solvent penetration, whereas PET's lower compatibility limits chain motion and solvent penetration.[32,33]

Characterization

FTIR. Cellulose structure in regenerated samples was evaluated using FTIR peak at 3300 – 3400 cm^{-1} (O-H stretch) and 875 cm^{-1} (β-glycosidic linkages) to determine preservation of cotton (Figure 4) While anti-solvent precipitation often induces a transition to cellulose II, the intensity profiles of the O-H and β-glycosidic peaks in the regenerated samples match those of pure cotton, confirming that the native cellulose I was successfully preserved. [34]

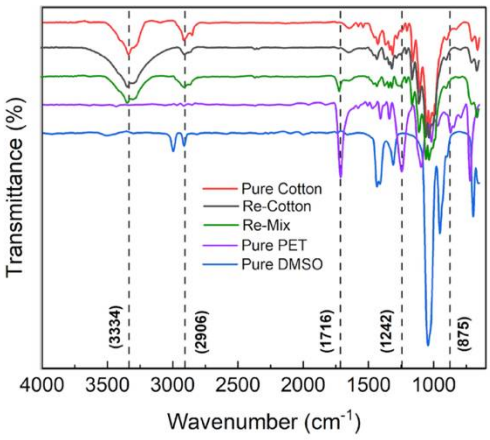


Figure 4. FTIR spectra of Pure Cotton, Pure PET, DMSO, Re-Cotton and Re-Mix.

The slight peak broadening observed in the O-H region reflects modified intermolecular hydrogen bonding and solvent-induced swelling rather than a complete crystal phase transition. For the Re-Mix sample, an additional peak at 1725 – 1710 cm^{-1} (C=O ester carbonyl) indicates trace of PET contamination, which slightly reduces chemical purity without compromising the cellulose backbone.[35] Preserving

the cellulose I structure is particularly beneficial, as it retains the higher mechanical strength and structural quality of native fibers required for high-value textile recycling.

TGA-DTG. Figure 5 presents TGA (a) and DTG (b) curves for Re-Cotton and Re-Mix, showing primary cellulose backbone degradation between 280 – 380 °C.[36] From the DTG curves, pure cotton exhibits a maximum decomposition temperature (T_{max}) of 365 ℃, while Re-Cotton shift to 374 ℃.[37] This 9 ℃ increases indicate enhanced thermal stability attributed to altered molecular packing and structural reorganization post-regeneration.[38]

Conversely, Re-Mix shows a reduced T_{max} of 357 ℃, pointing to increased structural heterogeneity and amorphous regions introduced during cotton/PET separation. These thermal trends correlate directly with structural characteristics identified via XRD and FTIR.

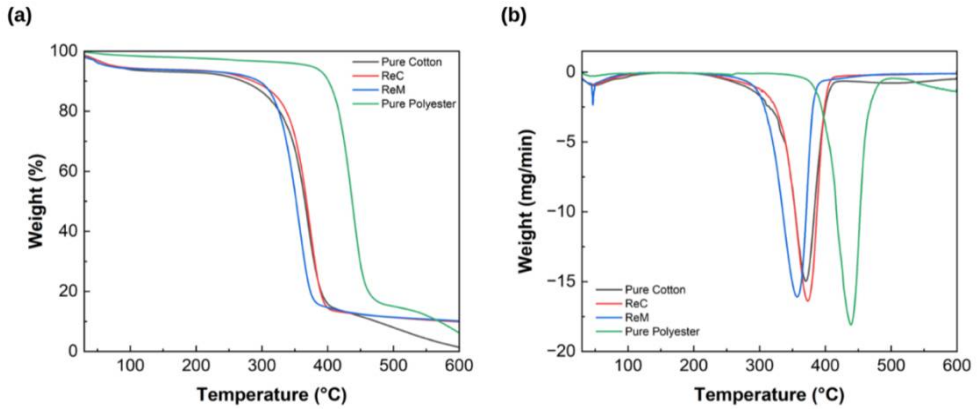


Figure 5. (a) TGA and (b) DTG thermal transitions curve of Pure Cotton, Pure PET, regenerated cotton from cotton-only samples (Re-Cotton), and regenerated cotton recovered from cotton/PET mixtures (Re-Mix).

SEM. Figure 6 shows images comparing untreated cotton (a-c) with regenerated cotton (Re-cotton) (d-f), and regenerated cotton from the blend

(Re-mix) (g-i). Both Re-Cotton (f) and Re-Mix (i) retain the characteristic smooth, flattened, ribbon-like morphology of native cotton fibers.[39] However, minor surface roughness is apparent in the regenerated samples, likely resulting from non-uniform coagulation and structural rearrangement during water precipitation. While maintaining macroscopic fiber shape confirms structural retention, SEM alone cannot verify full molecular dissolution vs partial dissolution with residual undissolved polymers. Thus, SEM findings were corroborated by XRD analysis, which confirmed preserved Cellulose I crystalline structure. Overall, DMSO processing and water anti-solvent precipitation alter surface structure while keeping primary cellulose features intact.[40,41]

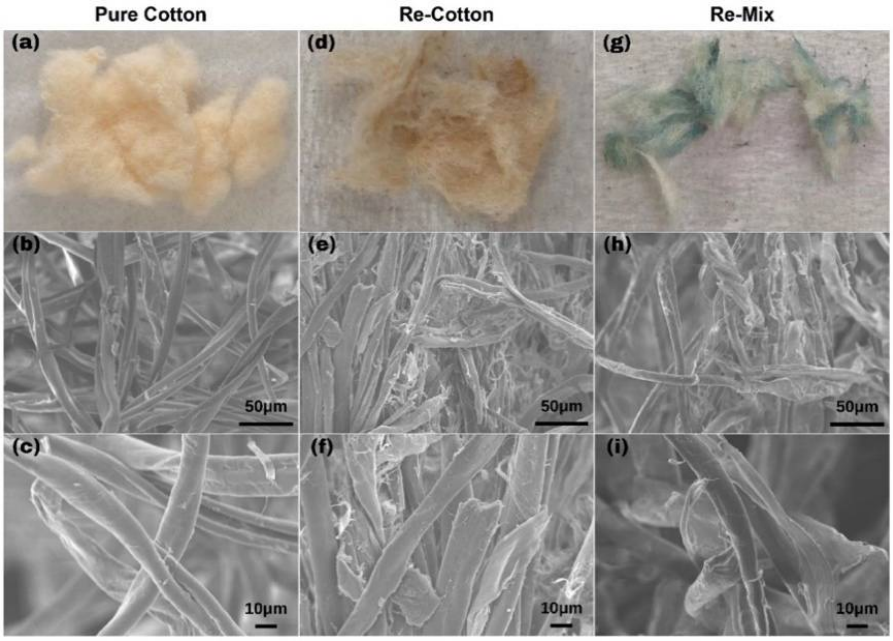


Figure 6. SEM micrographs of (a–c) pure cotton, (d-f) regenerated cotton (Re-Cotton), and (g-i) regenerated mixed fiber (Re-Mix) at magnifications 500x, and 1000x.

XRD and RDF. Figure 7(a) presents the XRD pattern of regenerated cotton recovered from DMSO/cellulose system. Diffraction peaks at 15.0°,

16.7°, 22.9°, and 34.9° confirm that native crystalline structure of native Cellulose I-like crystalline are retained post-regeneration. Relative to untreated cotton, a 3 – 4 % decrease in peak intensity and slight peak broadening point to a minor reduction in overall crystallinity. Compelementing XRD, the simulated radial distribution function (RDF) in Figure 7(b) tracks molecular-level intermolecular organization. Notably, RDF peaks reflect molecular pair-distance distribution rather than crystallographic lattice spacing. Together, XRD confirms preserved long-range Cellulose I domains, while RDF demonstrates retained short range intermolecular ordering. Thus, DMSO processing modifies crystalline order without disrupting the underlying Cellulose I framework, aligning with observation with Wei et al., Elf et al. and Zhang et al.[43,44,45]

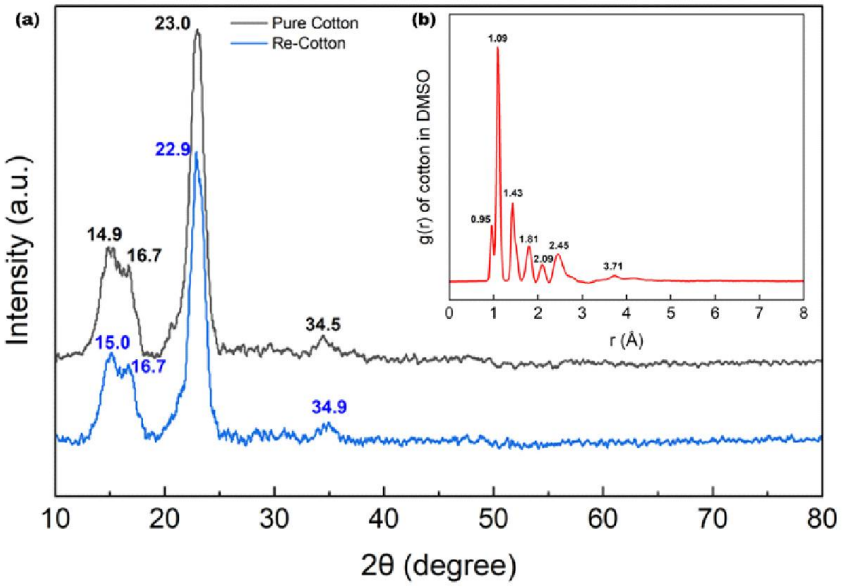


Figure 7. (a) XRD graph of Regenerated Cotton from cellulose/DMSO solution via water and (b) RDF graph of Interaction Cotton in DMSO by MD simulation.

Methodology

Materials

The interaction between polymer and solvent will be predicted using Materials Studio software (2023), developed by BIOVIA Dassault Systèmes that designated with 64 cores and 128 GB memory. Recycled cotton and PET fabrics will be obtained from the local market and decolourised using a 6% sodium hypochlorite (NaOCl, Chemiz) solution. The dissolution process will be carried out using DMSO (99.9%, Chemiz), and the fibres will be regenerated using distilled water. All chemicals were used without purification and purchased from BT Science Sdn Bhd (Selangor, Malaysia).

Molecular Dynamics (MD) Simulation

MD simulations were conducted in BIOVIA Materials Studio (2023) utilizing 64 CPU cores and 128 GB Ram. The setup workflow is depicted in Figure 8. Structural models of PET (ethylene terephthalate), cellulose (14 β-D-glucopyranose), and DMSO were retrived from the Cambridge Structural Database (CSD) (Figure 8(a)). Individual PET and cellulose chains were constructed from their repeating units (Figure 8(b)) where blue dashed line highlight hydrogen bonds. Each chain was packed into a 23 $Å^3$ using the Amorphous Cell module (Figure 8c) and geometry optimized using Forcite with the Smart Minimizer algorithm. The optimized chains were then combined with DMSO molecules in a 27 $Å^3$ simulation box at room temperature with 3.0 Å van der Waals cutoff distance size (Figure 8d).[46] Subsequent energy minimization via Forcite yielded stable low-energy structures (Figure 8(e)).

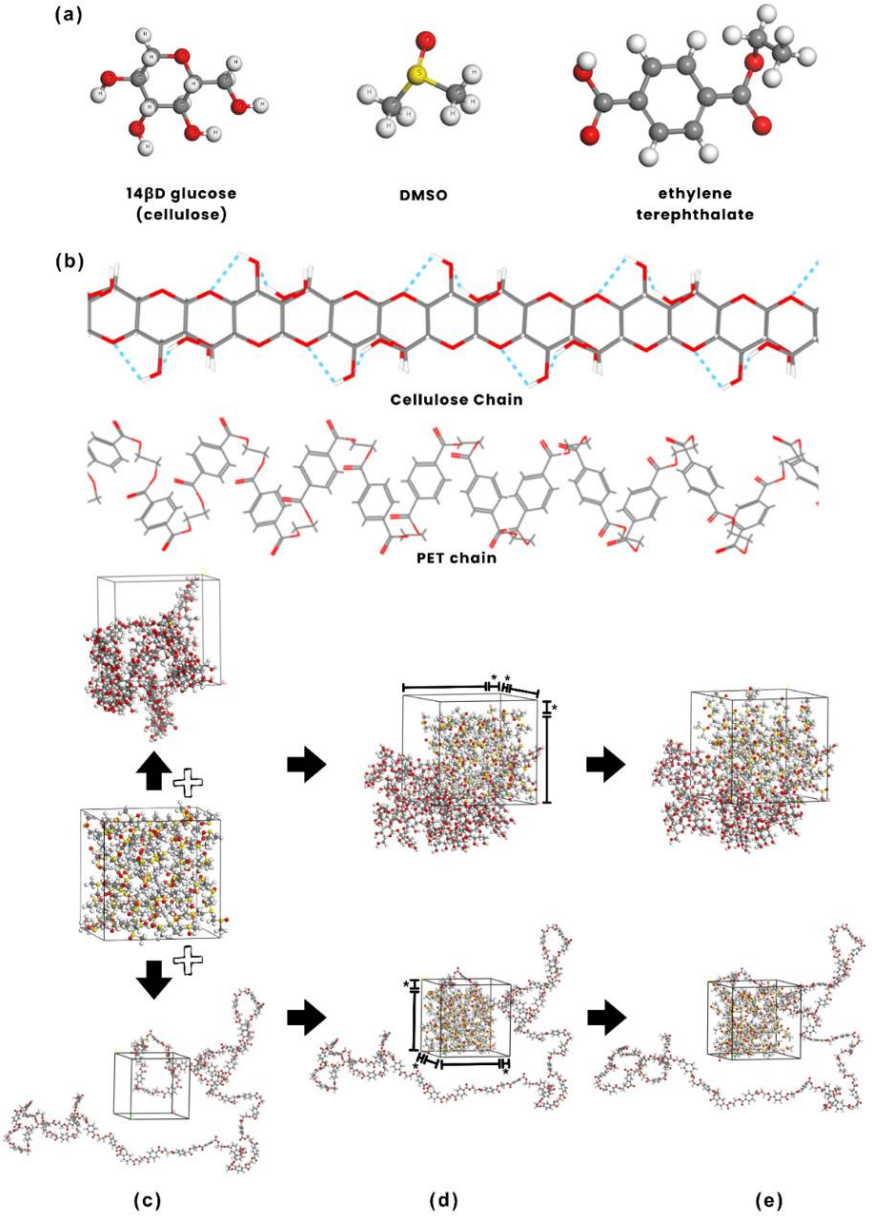


Figure 8. The example of procedural setup for geometry optimization step at 4.5mg/mL before procced to MD simulation. (a) The monomers of cotton, polyester and DMSO were imported from CSD, (b) The cellulose and PET chain segment (blue dashed line represents the hydrogen bond network), (c) A single chain of 30 repeating unit cotton and respective DMSO molecules were built in a separate cell (d) both molecules were combined into a cell with a tolerance distance of 3.0Å (*) from the original cell size and (e) The system's energy were optimized before proceed to MD simulation. All grey atom is the carbon, white atom is the hydrogen, red atom signifies the oxygen, and yellow atom is the sulfur.

As detailed in Table 3, a marked drop in total energy (E_{Total}) confirms that the constructed system achieved thermodynamic stability ready for equilibrium.

Table 3. The Total energy (E_{Total}) before and after energy optimization steps for each system at different concentration.

System	Concentration (mg/mL)	E_{Total} Before (kcal/mol)	E_{Total} After (kcal/mol)
PET/DMSO	4.5	2.59×10^{11}	7,167
	6.0	3.10×10^{11}	8,834
	7.5	3.63×10^{11}	9,104
Cellulose/DMSO	4.5	9.86×10^{11}	-1172
	6.0	13.35×10^{11}	-1033
	7.5	23.95×10^{11}	-857

Building on preliminary temperature studies, this work evaluated concentration effects (4.5, 6.0, 7.5 mg/mL) on polymer-solvent behaviour at optimized temperature of 423K.[47] Concentration was regulated by adjusting the chain length from eat initial value 50 repeating units via Equation 1.[48]

$$N_{adjusted} = N_{Initial} \times \frac{C_{desired}}{C_{reference}} \quad (1)$$

Post optimization, simulated densities for pure cellulose (1.330 g/cm^3) and PET (1.140 g/cm^3) closely matched experimental literature values.[37,46] The simulated cellulose density is lower than native crystalline cellulose Iβ (1.60 g/cm^3), capturing the disrupted, amorphous nature and reduced fibrillar packing of recycled cotton.[49] This low-density amorphous model accurately reflects the increased free volume and solvent accessibility inherent to dissolution.

These physical properties establish baseline references for concentration-dependent polymer-DMSO systems. Close agreement between simulated and experimental data confirms the validity of the

optimization method and force field parameters.[23] Key parameters for all polymer–DMSO systems are summarized in Table 4.

Table 4. The basic parameters of polymer and the combined polymer/DMSO system.

System	Concentration (mg/mL)	$N_{PET/Cellulose}$	N_{DMSO}	Density (g/cm^3)	Cell Size (Å^3)
PET/ DMSO	N/A	50	0	1.330	23
	4.5	30	121	1.340	27
	6.0	40	121	1.619	27
	7.5	50	121	1.722	27
Cellulose/ DMSO	N/A	50	0	1.140	23
	4.5	30	104	1.072	27
	6.0	40	104	1.370	27
	7.5	50	104	1.465	27

Following energy minimization, pre-equilibration was conducted under the the NPT ensemble to stabilize system density and temperature followed by 1 ns of production sampling in the NVT ensemble.[50] Temperature and pressure were controlled using the Andersen and Berendsen barostat, respectively. All atomic interactions were evaluated using COMPASS force field via equation 2.[2]

$$E_{total} = E_b + E_\theta + E_\varphi + E_\chi + E_{cross} + E_{ele} + E_{vdw} \quad (2)$$

where E_{total} is the total energy, E_b is bond stretching energy, and E_θ is angle bending energy. E_φ is dihedral torsion energy, E_χ is out-of-plane energy, E_{cross} is cross term interaction energy. Non bonded electrostatic interaction energy E_{elc}, and van der Waals E_{vdw} forces were computed using atom-based summation with a 12.5 Å cutoff. Thermodynamic and transport metrics-including interaction energy, binding energy, and mean squared displacement (MSD) and diffusion coefficient (D) was extracted using Forcite module. Non-bonded interaction energy and binding energy were defined according to Equations 3 and 4[46]:

$$E_{Interaction} = E_{Total} - (E_{Polymer} + E_{Solvent}) \quad (3)$$

$$E_{Binding} = -E_{Interaction} \quad (4)$$

As noted by Zhang et al., binding energy quantifies the energetic barrier to dislodging polymer chains during dissolution. Higher binding energies reflects stronger surface retention and slower dissolution kinetics, providing atomic-level insights into surface stability.[51] Furthermore, glass transition temperature Tg is strongly governed by polymer chain mobility, MSD tracks molecular diffusivity over time, with the slope pf the MSD curve characterizing distinct diffusion regimes.[52,53] As noted by Wanying Li et al., MSD seves as standard metric for evaluating polymer chain dynamics and is defined by Equation 5.[54]

$$MSD = \langle |r_i(t) - r_i(0)|^2 \rangle \quad (5)$$

where $r_i(t)$ is the coordinates of atom at time t, $r_i(0)$ is initial position of atoms in the system, and the angle bracket is the statistical average value of the time of the system under study MSD quantifies the average distance travelled by molecules or atoms over time, reflecting molecular mobility within a material. The diffusivity of molecules can be calculated using diffusion coefficient, D where the Eistein's relation for Brownian motion will be applied in equation (6):

$$D = \lim_{t \to \infty} \left(\frac{\langle |r_i(t) - r_i(0)|^2 \rangle}{6t} \right) \quad (6)$$

Higher MSD values reflect increased polymer chain mobility, which promotes dissolution. Additionally, the radial distribution function (RDF), g(r), was calculated between O_{DMSO} and $H_{Polymer}$ atoms to evaluate local structure and hydrogen-bonding behaviour. A sharp peak within 1.5 Å – 2.0 Å confirms strong hydrogen bonding between DMSO and polymer chains. Higher peak intensity and broader coordination shells indicate superior

solvent penetration, chain swelling, and enhanced dissolution within the polymer matrix. These computational predictions were experimentally validated using L9 Taguchi method.

Taguchi Design Method

Guided by MD simulation predictions, three experimental parameters (temperature, polymer concentration, and dissolution time) were evaluated using a L9 Taguchi orthogonal array (Table 5). Each factor assigned three operational levels based on preliminary testing: temperature (50 °C (Low), 100 °C (Mid), and 150 °C (High)), concentration (4.5 mg/mL (Low), 6.0 mg/mL (Mid), and 7.5 mg/mL (High)) and dissolution time (4 h (Low), 6 h (Mid), and 8 h (High)). This fractional factorial design allowed systematic assessment of individual parameter main effects on dissolution efficiency across 9 experimental runs.

Table 5. L9 Taguchi design showing different combinations of temperature, concentration, and reaction time used to study the dissolution of cotton and polyester in DMSO.

Exp No.	Temperature (℃)	Concentration (mg/mL)	Dissolution Time (h)
E1	50	4.5	4
E2	50	6.0	6
E3	50	7.5	8
E4	100	4.5	6
E5	100	6.0	8
E6	100	7.5	4
E7	150	4.5	8
E8	150	6.0	4
E9	150	7.5	6

Dissolution Process

Recycled textiles were decolorized in 0.6 M NaOCl using an ultrasonic bath (50 °C, 60 min), rinsed in distilled water for 5 min, and dried in a convection oven at 100 °C for 2 h. Dried fabrics were then pulverised

using a laboratory-scale grinder to achieve a fine powder with a particle size (~0.2 mm) (Figure 9).

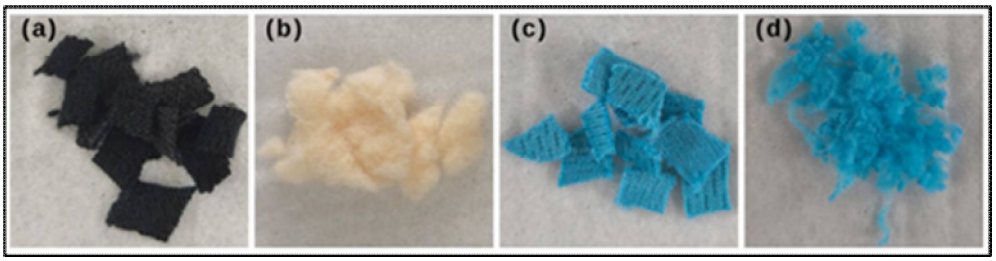


Figure 9. (a) Cotton before (b) Cotton after (c) Polyester before (d) Polyester after decolorization process with NaOCl.

The dissolution workflow is depicted in Figure 10.

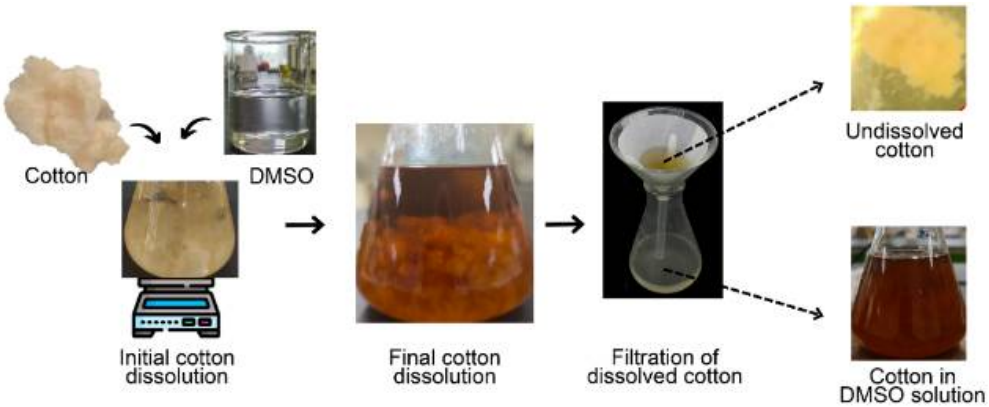


Figure 10. Dissolution process step using DMSO to separate dispersed cotton from filtrate.

Textile samples (Table 4) were first soaked in DMSO for 24 h at specified temperatures to promote solvent penetration, followed by continuous agitation at 500 rpm to facilitate dissolution. The mixture was filtered to separate undissolved cotton, and the cellulose-containing filtrate was treated with distilled as anti-solvent to induce precipitation. The regenerated cellulose precipitate was washed thoroughly with distilled water and oven-dried at 150°C for 2 h to yield a pure, solvent-free regenerated polymer which can be calculated using Equation 7.

$$D(\%) = \frac{\text{Initial Weight (mg)} - \text{Final Weight (mg)}}{\text{Initial Weight (mg)}} \times 100\% \quad (7)$$

Dissolution effectiveness was validated using Signal-to-Noise (S/N) ratio analysis under the "larger-the-better" criterion to maximize dissolution yield while minimizing process variability. Higher S/N ratio highlight optimal process conditions such as elevated temperatures and ideal concentrations that enhance dissolution performance while minimizing sensitivity to experimental noise factors.[28] Furthermore, a fixed-effects one-way analysis of variance (ANOVA) was performed to determine the statistical significance (F-values and P-values) of each parameter on overall dissolution efficiency.

Regeneration process

The regeneration step using water as anti-solvent is shown in Figure 11. The Following dissolution, the cotton/DMSO solution was cooled to 25 °C, and distilled water was added slowly to reach a 10:1 anti-solvent-to-solution volume ratio, following Leskinen et al.[56] The mixture was allowed to stand for 72 h to achieve complete precipitation. The regenerated fiber was washed three times with distilled water to remove residual DMSO and subsequently dried at 80℃ overnight.

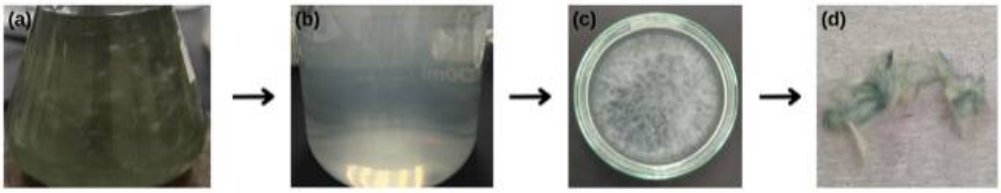


Figure 11. (a) The cotton/DMSO solution was cooled down to 25°C, (b) Add distilled water to achieve a 10:1 water-to-solution volume ratio, (c) Left the mixture for 72 hours until the cotton fiber fully precipitated and (d) Regenerated cotton fiber was slow dried at 80°C for overnight.

Characterization

The characterization study of structure changes in regenerated cotton was performed using Fourier-transform infrared spectrometer (FTIR,) spectroscopy, X-ray diffraction (XRD), thermogravimetric analysis (TGA) and scanning electron microscopy (SEM). FTIR spectra were obtained using a FTIR (Bruker VERTEX 70, German), averaging 32 scans over the 400 – 4000 cm^{-1} range. The crystalline structure of the regenerated cotton was examined using an XRD (SmartLab, Rigaku, Japan) operated at 40 kV and 30 mA. Diffraction patterns were collected over a 2θ range of 10° – 80° with a step size of 0.02°. The calculation of the interplanar spacing was using Bragg's law with Cu-Kα radiation (λ = 1.5406 Å). Thermal behaviour was analyzed by TGA (8000, Perkin Elmer, USA) under a nitrogen atmosphere (10 mL/min) to prevent oxidative degradation. Samples were heated from 25 °C to 350 °C at a constant rate of 10 °C/min. Morphological features of regenerated cotton were examined using SEM (JEOL JSM-IT200, Japan). Samples were mounted on aluminium stubs with conductive carbon tape and sputter-coated with approximately 5 nm of gold to enhance conductivity and resolution. Imaging was performed at an accelerating voltage of 10 kV with magnifications of 500x and 1000x.

Conclusions

This study established that cellulose exhibits significantly stronger thermodynamic interaction with DMSO than PET at interaction at 423 K with 4.5 mg/mL, highlighting the feasibility of selective polycotton separation. Experimental validation via L9 Taguchi orthogonal array confirmed optimal dissolution conditions at 150 ℃, 4.5mg/mL and 8 h, achieving high dissolution efficiency for cotton while leaving PET largely

intact. Testing was capped at 150 ℃ due to solvent degradation and retention consideration. Anti-solvent precipitation using water yielded regenerated cotton fibers that preserved their native crystallinity, functional group, and surface morphology. These results demonstrate that pure DMSO effectively separate polycotton blends without co-solvent while preserving the primary cellulose backbone. Overall, this work provides fundamental insights into polymer-DMSO interactions and offers a robust technical framework for developing scalable, solvent-based textile recycling processes.

Acknowledgements

Authors acknowledge the Ministry of Higher Education (MOHE) for funding under the Fundamental Research Grant Scheme (FRGS) (FRGS/1/2024/TK09/UITM/02/15) managed by Universiti Teknologi MARA (600-RMC/FRGS 5/3 (118/2024) for providing the facilities and resources necessary for this research.

Conflicts of interest

The authors declare that they have no known competing financial interests or personal relationships associated with this work.

References

1. Miyata, T.; Funahara, Y.; Omori, S. and Shinjo, T. A study on the extension of correlation functions obtained from molecular dynamics simulations by the Ornstein–Zernike theory for modeled molten salts. *AIP Adv.* **2023**, *13*(11), 115322. https://doi.org/10.1063/5.0180366

2. Bazooyar, F.; Momany, F. A. and Bolton, K. Validating empirical force fields for molecular-level simulation of cellulose dissolution. *Comput. Theor. Chem.* **2012**, *984*, 119 – 127. https://doi.org/10.1016/j.comptc.2012.01.020

3. Yan, Z.; Lian, J.; Li, M.; Meng, L.; Zhang, Y.; Ge, C. and Lu, J. Deeper insight into hydrolysis mechanisms of polyester/cotton blended fabrics for separation by explicit solvent models. *Int. J. Biol. Macromol.* **2020**, *154*, 596 – 605. https://doi.org/10.1016/j.ijbiomac.2020.03.130

4. Wu H.; Wang, B.; Li, T.; Wu, Y.; Yang; R., Gao, H. and Nie, Yi. Efficient recycle of waste poly-cotton and preparation of cellulose and polyester fibers using the system of ionic liquid and dimethyl sulfoxide. *J. Mol. Liq.* **2023**, *388*, 122757. https://doi.org/10.1016/j.molliq.2023.122757

5. Lee, H. L.; Yang, C. L. and Lee, T. Shaping particle size distribution of a metastable polymorph in additive-assisted reactive crystallization by the Taguchi method. *Cryst. Eng. Comm*. **2022**, *24*(40), 7176 – 7192. https://doi.org/10.1039/d2ce00355d

6. Mensah, R. A.; Kirton, S. B.; Cook, M. T.; Styliari, I. D.; Hutter, V. and S. Chau, D. Y. Optimising poly(lactic-co-glycolic acid) microparticle fabrication using a Taguchi orthogonal array design-of-experiment approach. *PLoS One* **2019**, *14*(9), e0222858. https://doi.org/10.1371/journal.pone.0222858

7. Lee, I. and Yang, N. -C. Using taguchi method to determine the optimum conditions for synthesizing parapyruvate. *Molecules* **2022**, *27*(6), 1870. https://doi.org/10.3390/molecules27061870

8. Baloyi, R. B.; Gbadeyan, O. J.; Sithole, B. and Chunilall V. Recent advances in recycling technologies for waste textile fabrics: a review. *Tex. Res. J.* **2024**, *94*(3-4), 508 – 529. https://doi.org/10.1177/00405175231210239

9. Singhal, S.; Agarwal, S. and Singhal, N. Chemical recycling of waste clothes: a smarter approach to sustainable development. *Environ. Sci. Pollut. Res.* **2023**, *30*(1), 54448 – 54469. https://doi.org/10.1007/s11356-023-26438-y

10. Ren, F.; Wang, J.; Yu, J.; Zhong, C.; Xie, F. and Wang, S. Dissolution of cellulose in ionic liquid–DMSO mixtures: roles of DMOS/IL ratio and the cation alkyl chain length. *ACS Omega* **2021**, *6*(41), 27225 – 27232. https://doi.org/10.1021/acsomega.1c03954

11. André, A. D.; Teixeira, A. M. and Martins, P. Influence of DMSO non-toxic solvent on the mechanical and chemical properties of a PVDF thin film. *Appl. Sci*. **2024**, *14*(8), 3356. https://doi.org/10.3390/app14083356

12. Reuter, H. Structural parameters of dimethyl sulfoxide, DMSO, at 100 K, based on a redetermination by use of high-quality single-crystal X-ray data. *Acta Crystallogr. E Crystallogr. Commun*. **2017**, *73*(10), 1405 – 1408. https://doi.org/10.1107/S2056989017012464

13. Marino, T.; Galiano, F.; Simone, S. and Figoli, A. DMSO EVOLTM as novel non-toxic solvent for polyethersulfone membrane preparation. *Environ. Sci. Pollut. Res*. **2019**, *26*(15), 14774 – 14785. https://doi.org/10.1007/s11356-018-3575-9

14. Cimatu, K. L. A.; Ambagaspitiya, T. D.; Premadasa, U. I; Adhkari, N. M.; Kruse, A.; Robertson, E., Guan, S.; Rong, L.; Advincula, R. and Bythell, B. J. Polymer-solvent interaction and conformational changes at a molecular level: Implication to solvent-assisted deformation and aggregation at the polymer surface. *J. Colloid Interface Sci*. **2022**, *616*, 221 – 233. https://doi.org/10.1016/j.jcis.2022.02.006

15. Danner, R. P. and High, M. S. Handbook of polymer solution thermodynamics. Wiley, **1993**. https://doi.org/10.1002/9780470938232.fmatter

16. Gelpi, J.; Hospital, A.; Goñi, R. and Orozco M. Molecular dynamics simulations: advances and applications. *Adv. Appl. Bioinform. Chem.* **2015**, *8*, 37 – 47. https://doi.org/10.2147/AABC.S70333

17. Grzybek, P.; Dudek, G. and van der Bruggen, B.; Cellulose-based films and membranes: A comprehensive review on preparation and applications. *Chem. Eng. J.* **2024**, *495*, 153500. https://doi.org/10.1016/j.cej.2024.153500

18. Hayakawa, D.; Nishiyama, Y.; Mazeau, K. and Ueda, K. Evaluation of hydrogen bond networks in cellulose Iβ and II crystals using density functional theory and Car–Parrinello molecular dynamics. *Carbohydr. Res.* **2017**, *449*, 103 – 113. https://doi.org/10.1016/j.carres.2017.07.001

19. Verma, J.; Petru, M. and Goel, S. Cellulose based materials to accelerate the transition towards sustainability, *Ind. Crops Prod.* **2024**, *210*, 118078. https://doi.org/10.1016/j.indcrop.2024.118078

20. Wang, X.; Zheng, W.; Guo, Z.; Nawaz, H.; You, T.; Li, X. and Xu, F. Rheological characteristics of novel cellulose/superbase-derived ionic liquid solutions and the coagulation process towards regenerated cellulose films. *Green Chem.* **2023**, *25*(4), 1597 – 1610. https://doi.org/10.1039/d2gc03278c

21. Taheri, N.; Abdolmaleki, A. and Fashandi, H. Impact of non-solvent on regeneration of cellulose dissolved in 1-(carboxymethyl)pyridinium chloride ionic liquid. *Polym. Int.* **2019**, *68*(12), 1945 – 1951. https://doi.org/10.1002/pi.5903

22. Parviainen, A.; Wahlstrom, R.; Limatainen, U.; Litia, T.; Rovio, S.; J. Helminen, J. K.; Hyväkkö, U.; King, A. W. T.; Suurnäkki, A. and Kilpeläinen I. Sustainability of cellulose dissolution and regeneration in 1,5-diazabicyclo[4.3.0]non-5-enium acetate: a batch simulation of the IONCELL-F process. *RSC Adv.* **2015**, *5*(85), 69728 – 69737. https://doi.org/10.1039/c5ra12386k

23. Zheng, J.; Wang, D.; Zhang, Q.; Song, M.; Jiao, M. and Zhang, Z. Molecular dynamics simulation and structure changes of polyester in water and non-aqueous solvents. *Materials* **2022**, *15*(6), 2148. https://doi.org/10.3390/ma15062148

24. Muhammad Faez Tan, N. U. W.; Muhammad, A.; Abu Bakar, N. F.; Azmi, I. S. and Roslan, A. Molecular dynamics simulation study on the effect of temperature during dissolution cellulose and polyester (textile waste) in dimethyl sulfoxide, in *Proceedings of the 9th International Conference on Fuel Cell & Hydrogen Technology*, ICFCHT **2025**, 10-11Sept., Kuala Lumpur, Malaysia; Aishah Abdul Jalil, Rafiziana Md. Kasmani, and Roshafima Rasit Ali, Eds., Springer Proceedings in Physics, *in press*, 2026.

25. Maria, I. P.; Paulsen, B. D.; Savva, A.; Ohayon, D.; Wu, R.; Hallani, R.; Basu, A.; Du, W.; Anthopoulos, T. D.; Inal, S.; Rivnay, J.; McCulloch, I. and Giovannitti, A. The effect of alkyl spacers on the mixed ionic-electronic conduction properties of n-type polymers. *Adv. Funct. Mater.* **2021**, *31*, 2008718. https://doi.org/10.1002/adfm.202008718

26. Yong L, Jian L, Xian L, Bei W. Test and analysis of the porosity of cotton fiber assembly. *J. Eng. Fiber. Fabr.* **2021**, *16*, 508 – 529. https://doi.org/10.1177/15589250211024225

27. Angelotti, A.; Alongi, A.; Augello, A.; Dama, A.; Antonellis, S. D.; Ravidà, A.; Zinzi, M.; Angelis, E. D. Thermal conductivity assessment of cotton fibers from apparel recycling for building insulation. *Energy Build.* **2024**, 324, 114866. https://doi.org/10.1016/j.enbuild.2024.114866

28. Jiang, X.; Wang, W.; Guo, Y. and Dai, M. Molecular dynamics simulation of the effect of low temperature on the properties of lignocellulosic amorphous region. *Forests* **2023**, *14*(6), 1208. https://doi.org/10.3390/f14061208

29. Najib, M.; Hammond, R. B.; Mahmud, T. and Izumi, T. Impact of structural binding energies on dissolution rates for single faceted-crystals, *Cryst. Growth Des.* **2021**, *21*(3), 1482 – 1495. https://doi.org/10.1021/acs.cgd.0c01142

30. Suter, J. L.; Müller, W. A.; Vassaux, M.; Anastasiou, A.; Simmons, M.; Tilbrook, D. and Coveney, P. V. Rapid, accurate and reproducible prediction of the glass transition temperature using ensemble-based molecular dynamics simulation, *J. Chem. Theory Comput.* **2025**, *21*(3), 1405 – 1421. https://doi.org/10.1021/acs.jctc.4c01364

31. Deckers, F.; Rasim, K. and Schröder, C. Molecular dynamics simulation of polypropylene: diffusion and sorption of H_2O, H_2O_2, H_2, O_2 and determination of the glass transition temperature. *J. Polym. Res.* **2022**, *29*(11), 463. https://doi.org/10.1021/acs.jctc.4c01364

32. Li, W.; Ma, J.; Wu, S.; Zhang, J. and Cheng, J. The effect of hydrogen bond on the thermal and mechanical properties of furan epoxy resins: Molecular dynamics simulation study. *Polym. Test.* **2021**, *101*, 107275. https://doi.org/10.1016/j.polymertesting.2021.107275

33. Lin L. and Tsuchii K. Dissolution behavior of cellulose in a novel cellulose solvent. *Carbohydr. Res.* **2022**, *511*, 108490. https://doi.org/10.1016/j.carres.2021.108490

34. Leskinen, M.; Mirzaei, Z.; Kemell, M.; Kilpeläinen, I. and Aseyev, V. Formation of core–shell structures and viscous fingering in cellulose beads regenerated from [DBNH][OAc]/DMSO. *Cellulose* **2024**, *31*(17), 10253 – 10269. https://doi.org/10.1007/s10570-024-06217-9

35. Wang, B.; Gao, H.; Wu, H.; Wu, Y.; Ren, B.; Liu, X.; Nie, Y. Diffusion coefficients during regenerated cellulose fibers formation using ionic liquids as solvents: Experimental investigation and molecular dynamics simulation. *Chem. Eng. J.* **2024**, *488*, 151175. https://doi.org/10.1016/j.cej.2024.151175

36. Xiang, J.; Gao, Q. and Wu, A. The Applications of DMSO. In *Solvents as Reagents in Organic Synthesis*, X.-F.W. Wu Ed.; Wiley, **2017**, 315 – 353. https://doi.org/10.1002/9783527805624.ch7

37. Cheng, X.; Ye, H.; Guo, C.; Pan, L. and Lu, L. Molecular dynamics simulation of the effects of intermolecular interactions on the diffusion mechanism of 1,2,3-benzotriazole in low density polyethylene. *J. Polym. Res.* **2024**, *31*(4), 109. https://doi.org/10.1007/s10965-024-03961-1

38. Saba, H.; Yongbo, Y.; Jianning, W.; Xiaolin, X.; Kaijian, W.; Yumei, Z. and Huaping, W. Effect of dimethylsulfoxide on the viscoelastic properties and sol–gel transition of cellulose/ionic liquid solutions, *RSC Adv*. **2015**, *5*(11), 8318 – 8322. https://doi.org/10.1039/c4ra14911d

39. Etale, A.; Onyianta, A. J.; Turner, S. R. and Eichhorn, S. J. Cellulose: A review of water interactions, applications in composites, and water treatment. *Chem. Rev.* **2023**, *123*(5), 2016 – 2048. https://doi.org/10.1021/acs.chemrev.2c00477

40. Kirshanov, K.; Toms, R.; Aliev, G.; Naumova, A.; Melnikov, P. and Gervald A. Recent developments and perspectives of recycled poly(ethylene terephthalate)-based membranes: A review. *Membranes (Basel)* **2022**, *12*(11), 1105. https://doi.org/10.3390/membranes12111105

41. Sfameni, S.; Lawnick, T.; Rando, G.; Visco, A.; Textor, T. and Plutino, M. R. Super-hydrophobicity of polyester fabrics driven by functional sustainable fluorine-free silane-based coatings. *Gels* **2023**, *9*(2), 109. https://doi.org/10.3390/gels9020109

42. Szafran, K.; Jurak, M.; Mroczka, R. and Wiącek, A. E. Surface properties of the polyethylene terephthalate (PET) substrate modified with the phospholipid-polypeptide-antioxidant films: design of functional biocoatings. *Pharmaceutics* **2022**, *14*(12), 2815. https://doi.org/10.3390/pharmaceutics14122815

43. Primc G. and Mozetič, M. Hydrophobic recovery of plasma-hydrophilized polyethylene terephthalate polymers. *Polymers (Basel)* **2022**, *14*(12), 2496. https://doi.org/10.3390/polym14122496

44. Wu, J.; Zhong, Y.; Kang, H. and Liu, R. Mechanism of dissolution of cellulose in quaternary ammonium phosphate/dimethyl sulfoxide. *Carbohydr. Polym.* **2025**, *352*, 123167. https://doi.org/10.1016/j.carbpol.2024.123167

45. Keppeler, N.; Augusto P.; Pires, R.; Leandro J.; Freitas, S. and El Seoud, O. A. Cellulose dissolution in mixtures of ionic liquids and molecular solvents: The fruitful synergism of experiment and theory. *J. Mol. Liq*. **2023**, *386*, 122490. https://doi.org/10.1016/j.molliq.2023.122490

46. Xu, A.; Chen, L.; Wang, Y.; Liu, R. and Niu, W. Development of diallylimidazolium methoxyacetate/DMSO (DMF/DMA) solvents for improving cellulose dissolution and fabricating porous material. *Polymers (Basel)* **2019**, *11*(5), 845. https://doi.org/10.3390/polym11050845

47. Leenders, N.; Moerbeek, R. M.; Puijk, M. J.; Bronkhorst, R. J.; Moron, J. B; Klink, G.P.M and Gruter, G.M, Polycotton waste textile recycling by sequential hydrolysis and glycolysis. *Nat. Commun.* **2025**, *16*(1), 738. https://doi.org/10.1038/s41467-025-55935-6

48. Liu, W.; Liu, S.; Liu, T.; Liu, T.; Zhang, J. and Liu, H. Eco-friendly post-consumer cotton waste recycling for regenerated cellulose fibers. *Carbohydr. Polym.* **2019**, *206*, 41 – 148. https://doi.org/10.1016/j.carbpol.2018.10.046

49. Sankauskaite, A.; Stygiene, L.; Tumeniene, M. D.; Krauledas, S.; Jovaišiene, L. and Puodžiuniene, R. Investigation of cotton component destruction in

cotton/polyester blended textile waste materials. *Medziagotyra* **2014**, *20*(2), 189 – 192. https://doi.org/10.5755/j01.ms.20.2.3115

50. Lai, V. W. X.; Jamaluddin, J.; Mat Nasir, N. A. F.; Baharulrazi, N.; Majid, R. A.; Lai, J. C.; Mohd Bohari, S. P.; Chua, L. S.; Hasham, R.; Rahmat, Z. and Adrus N. Extraction of cellulose from rice straw for regeneration of hydrogels. *Environ. Qual. Manag.* **2022**, *32*(1), 333 – 341. https://doi.org/10.1002/tqem.21825

51. Hou, W.; Ling, C.; Shi, S; Yan, Z.; Zhang, M.; Zhang, B. and Dai, J. Separation and characterization of waste cotton/polyester blend fabric with hydrothermal method. *Fibers Polym.* **2018**, *19*(4), 742 – 750. https://doi.org/10.1007/s12221-018-7735-9

52. Basch, A. and Lewin, M. The Influence of fine structure on the flame retardance of cellulose. *Tex. Res. J.* **1975**, *45*(3), 246 – 250. https://doi.org/10.1007/s12221-018-7735-9

53. Ramana, C. V.; Makeswaran, N.; Zade, V.; Das, D.; Tan, S.; Xu, S. and Beyerlein, I. J. Fabrication and characterization of high-quality epitaxial nanocolumnar niobium films with abrupt interfaces on YSZ(001). *J. Phys. Chem.* C **2022**, *126*(4), 2098 – 2107. https://doi.org/10.1021/acs.jpcc.1c08738

54. Wei, J.; Long, Y.; Li, T.; Gao, H. and Nie, Y. Exploring hydrogen-bond structures in cellulose during regeneration with anti-solvent through two-dimensional correlation infrared spectroscopy. *Int. J. Biol. Macromol.*, **2024**, *267*, 131204. https://doi.org/10.1016/j.ijbiomac.2024.131204

55. Elf, P.; Özeren, H. D.; Larsson, P. A.; Larsson, A.; Wågberg, L.; Nilsson, R.; Chaiyupatham, P. T.; Hedenqvist, M. S. and Nilsson F. Molecular dynamics simulations of cellulose and dialcohol cellulose under dry and moist conditions. *Biomacromolecules* **2023**, *24*(6), 2706 – 2720. https://doi.org/10.1021/acs.biomac.3c00156

56. Zhang, X.; Zhou, W.; Xing, W.; Xu, Y. and Zhang, G. Efficient recovery of waste cotton fabrics using ionic liquid methods. *Polymers (Basel)* **2025**, *17*(7), 900. https://doi.org/10.3390/polym17070900